Geometry Optimization for Miniaturized Thermoelectric Generators

Gustavo G. Dalkiranis,* João H. C. Bocchi, Osvaldo N. Oliveira, Jr., and Gregório C. Faria

Read Online

ACCESS | Metrics & More | Article Recommendations | Supporting Information

ABSTRACT: Thermoelectric materials capable of converting heat into electrical energy are used in sustainable electric generators, whose efficiency has been normally increased with incorporation of new materials with high figure of merit (ZT) values. Because the performance of these thermoelectric generators (TEGs) also depends on device geometry, in this study we employ the finite element method to determine optimized geometries for highly efficient miniaturized TEGs. We investigated devices with similar fill factors but with different thermoelectric leg geometries (filled and hollow). Our results show that devices with legs of hollow geometry are more efficient than those with filled geometry for the same length and cross-sectional area of thermoelectric legs. This behavior was observed for thermoelectric leg lengths smaller than 0.1 mm, where the leg shape causes a significant difference in temperature distribution along the device. It was found that for reaching highly efficient miniaturized TEGs, one has to consider the leg geometry in addition to the thermal conductivity.
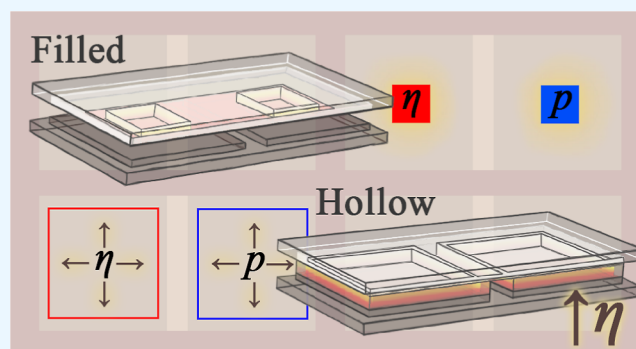
1. INTRODUCTION

The search for technologies to allow humankind to harvest energy from renewable sources is crucial to reduce global warming and partially solve the energy crisis.[1,2] While photovoltaic and wind power technologies are already maturing and available in the market, the same does not apply to technologies for harvesting heat waste. These technologies may positively impact the energetic matrix[3] since roughly 60% of the energy obtained is wasted as heat in industrial or domestic processes.[4] This energy harvesting may also be obtained with microgenerators to power wearable devices, smart fabrics, and small medical gadgets, such as pacemakers.[5–10] In this context, thermoelectric generators (TEGs) which transform thermal energy (heat) into electrical energy can be used to recover part of the energy lost in heat form.[11–13] These are devices with two (or more) thermoelectric legs, one p-type and the other n-type, thermally connected in parallel and electrically in series, named as thermocouples.[14–16] Figure 1 shows a simplified scheme of a thermoelectric generator (TEG).

The capacity of a thermoelectric generator to convert heat into electrical energy is given by the figure of merit (ZT) defined using eq 1[17]

$$ZT = \frac{S_{device}^2}{R_{device}G_{device}}T_{avg} \qquad (1)$$

where S_{device} is the Seebeck coefficient, T_{avg} is the average temperature between the temperature of the hot (T_H) and cold (T_C) sides, R_{device} is the internal electrical resistance, and G_{device} is the thermal conductance of the device. Since the geometric
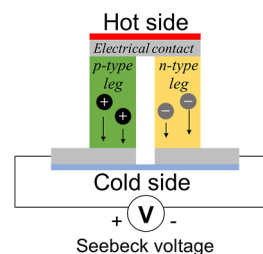

Figure 1. Thermoelectric generator with two thermoelectric legs. The displacement of the charge carriers is caused by the temperature gradient.

terms in the thermal and electrical conductivities cancel each other out, eq 1 can be written from $ZT = \frac{S^2\sigma}{k}T$.[17] Because the Seebeck coefficient and electrical and thermal conductivities can depend on the temperature, this equation is not always valid, especially with high temperature differences.[18] Throughout this article, however, we will keep the temperature gradient not higher than 4 K, which is within the reliability of eq 1. Since a thermoelectric generator is basically a heat engine converting heat into electrical energy to perform work, its
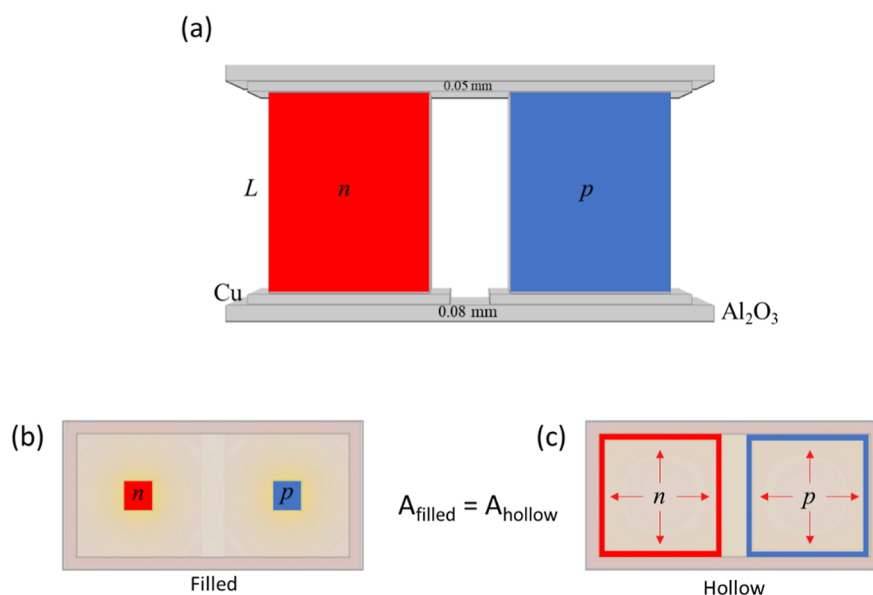
Figure 2. (a) Scheme of TEG geometries used in the simulations. A top view of the thermoelectric leg geometries in the cases: filled (b) and hollow (c).

efficiency is limited by the Carnot cycle efficiency, corrected by a reducing thermoelectric factor. It can be calculated using eq 2[14−16,19,20]

$$\eta_{TE} = \frac{T_H - T_C}{T_H} \frac{\sqrt{1 + ZT} - 1}{\sqrt{1 + ZT} + \frac{T_C}{T_H}} \qquad (2)$$

where T_H and T_C are the temperatures of the hot and cold sides, respectively. Therefore, for a fixed T_H and T_C, the higher the ZT, the higher the efficiency is. It is worth mentioning that the COMSOL's thermoelectric module considers temperature-dependent material parameters and the Thomson effect. Therefore, the heat flux parameter calculated in our modeling protocol considers the Thomson effect, validating the use of eq 2 to calculate the overall device efficiency. Several strategies have been reported to increase the efficiency (η_{TE}), ranging from synthesizing new materials to producing hybrid devices.[21,22] The most common route, however, is still the search for new materials and composites with high ZT values.[23−28] Nonetheless, it is known that the overall device geometry can play an important role on the properties of electrical and thermal systems.[29−31] Of great interest here is the optimization of the geometry of the thermoelectric legs.[32] For instance, when reducing the length of the thermoelectric legs to about 55% of their original size, there was a 10% increase in the conversion efficiency and a 48% increase in the output efficiency.[33] It is clear that longer thermoelectric legs increase the overall thermal resistance, thus decreasing thermal conductance. A reduction in thermal conductance is normally desirable to ensure that the temperature difference between the leg extremes is preserved and optimized. For automobile waste heat recovery, Kumar et al. observed that the efficiency of thermoelectric legs depends on their length, with optimization of the length and filling fraction yielding a maximum output power even reducing the amount of material used.[34] On the other hand, the longer the leg, the higher the internal resistance is, negatively impacting the efficiency. This en passant analysis suggests that there will be an optimal value for the length of the devices, revealing the importance of device

geometry to the thermoelectric efficiency. Additional strategies are used to increase the temperature gradient without negatively affecting other device parameters. Glatz et al. studied the thermal resistance between the thermal and electrical contacts, suggesting that it could be optimized to enhance the temperature gradient between the thermoelectric legs.[29] The group of Professor LeBlanc explored several leg shapes and their influence on the power output of TEGs. Although some of the shapes are difficult to realize experimentally, their work confirmed the importance of leg geometry on optimized TEGs.[30,31] A thorough review on this topic brought a compilation of results, in which device geometries are correlated with the thermoelectric efficiency and power output.[32]

Here, we focused on understanding the influence of the thermoelectric leg geometry on miniaturized TEG parameters. Simulations with the thermoelectric module of COMSOL software were carried out for two types of thermoelectric leg geometries, as shown in Figure 2, i.e., filled and hollow. They had similar cross-sectional areas, and a fixed temperature gradient was applied to the devices. The device efficiency was calculated varying the length and cross-sectional area of the thermoelectric legs. Our results indicate that for a leg length smaller than 0.1 mm, its shape affects the TEG efficiency by changing the temperature profile along the device. Furthermore, we present guidelines for constructing optimized miniaturized TEGs, considering that the temperature distribution along the device depends not only on the thermal conductance but also on the leg geometry.

2. MODELING

The influence of leg geometry on the TEG efficiency was studied with two geometries for the thermoelectric legs: (a) filled (Figure 2b) and (b) hollow (Figure 2c). The cross-sectional area (fill factor) and length (L) were varied for both geometries to allow for a comparison. The simulations were performed using a device with two thermoelectric legs of p- and n-type Bi_2Te_3, with electrical and thermal contacts of copper and Al_2O_3, respectively. The electrical and thermal
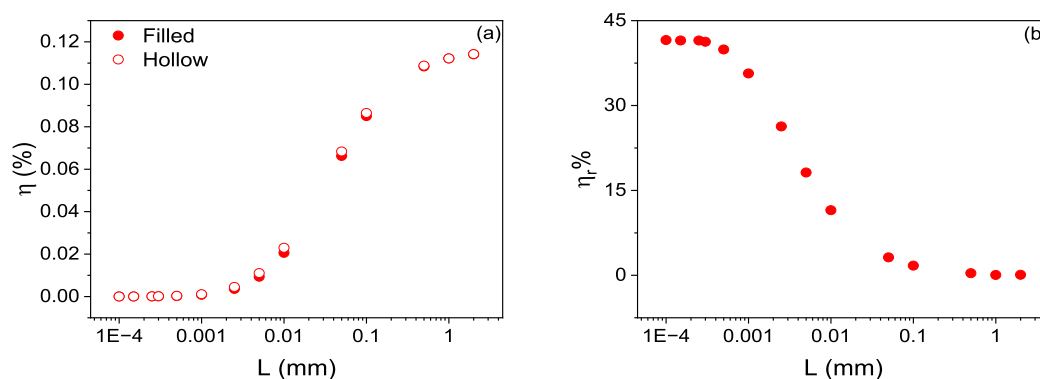
Figure 3. (a) Efficiency of TEGs with filled and hollow thermoelectric leg geometries as a function of the length of the thermoelectric leg. (b) Relative increase percentage in the TEG efficiency for the hollow compared with the filled case.
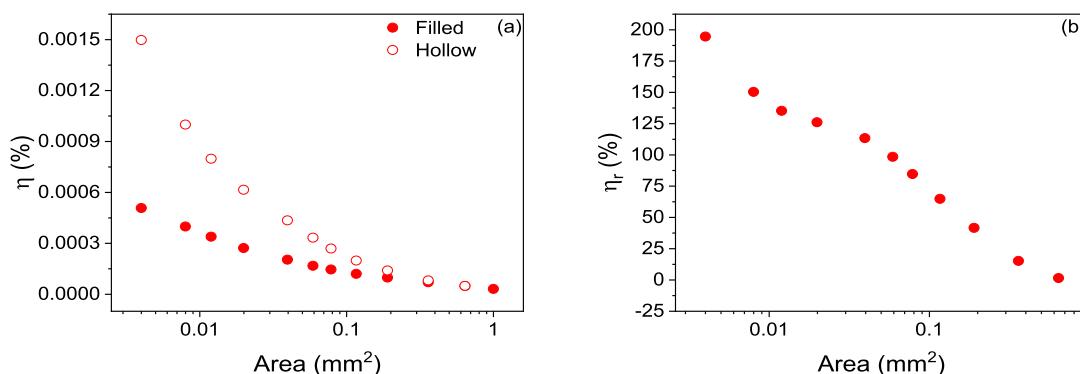

Figure 4. (a) TGE efficiency for hollow and filled thermoelectric legs as a function of the cross-sectional area. (b) Relative increase percentage in the TEG efficiency for the hollow compared with the filled case.

contact resistances between the thermoelectric legs and the electrical contacts were considered in the model according to the experimental values.[35,36] All the physical parameters at 300 K are summarized in Table S1 in the Supporting Information. We have used the temperature-dependent physical parameters from the COMSOL database. Figure 2a presents the overall scheme of the simulated TEG geometries. The calculation of the figure of merit (ZT) requires the Seebeck coefficient (S), thermal conductance (G), and internal resistance (R) of the device, which were obtained using the thermoelectric module of COMSOL software. The Seebeck coefficient and thermal conductance were obtained simultaneously, within the same calculation run. A temperature difference ($\Delta T = 302 - 298 = 4$ K) was applied to the borders of the device (between the hot and cold sides) to calculate the Seebeck voltage (V_S). The Seebeck coefficient was calculated by dividing the generated Seebeck voltage by the temperature difference applied to the device ($S = V_S/\Delta T$). Throughout the simulation process, the device was considered as thermally isolated and under vacuum, transferring heat only through thermal contact. To determine the thermal conductance (G), the cross-sectional heat flux (ϕ_q) through the copper contact to the thermoelectric legs was probed (in W/m^2). Thermal conductance was calculated using eq 3

$$G = \frac{\phi_q A}{\Delta T} \qquad (3)$$

The TEG internal electrical resistance was obtained with a 10 μA direct current feeding the device, and the electric potential in each electrical contact (Cu) was probed. This

resistance was determined using Ohm's law, $R = \frac{V_1 - V_2}{i}$. Due to the low electric current applied, the internal electrical resistance was attained at 300 K, and an assumption was made of a uniform temperature along the thermoelectric legs. In subsidiary simulations, a temperature difference in the thermoelectric legs was considered, but there was no significant influence on the results (see Table S2 in the Supporting Information). The internal resistances were calculated assuming a temperature gradient ($T_{varying}$) and without the temperature gradient (T_{fixed}). The difference in resistance between the two conditions is smaller than 1.4%, justifying the use of a fixed internal resistance. Therefore, we assumed no change in temperature to calculate the internal resistance, reducing the computational cost. In addition, the steady-state analysis in all the simulations considered the heat conduction through the thermoelectric leg, as well as the electric potential generated by the leg due to the Seebeck effect. Fourier's law determines the heat conduction mentioned above through the equation

$$\vec{q} = -k\nabla T \qquad (4)$$

where $\overline{q}$ is the conductive heat flux vector, k is the thermal conductivity of the material, and ∇T is the temperature gradient. Using the Seebeck relationship, the electric potential at each point can be calculated, thus

$$\vec{E} = S \times \vec{\nabla} T \qquad (5)$$

where $\overline{E}$ is the vector of the electric field intensity, S is the Seebeck coefficient, and T is the temperature. For further details, we refer readers to the work by the group of Prof.
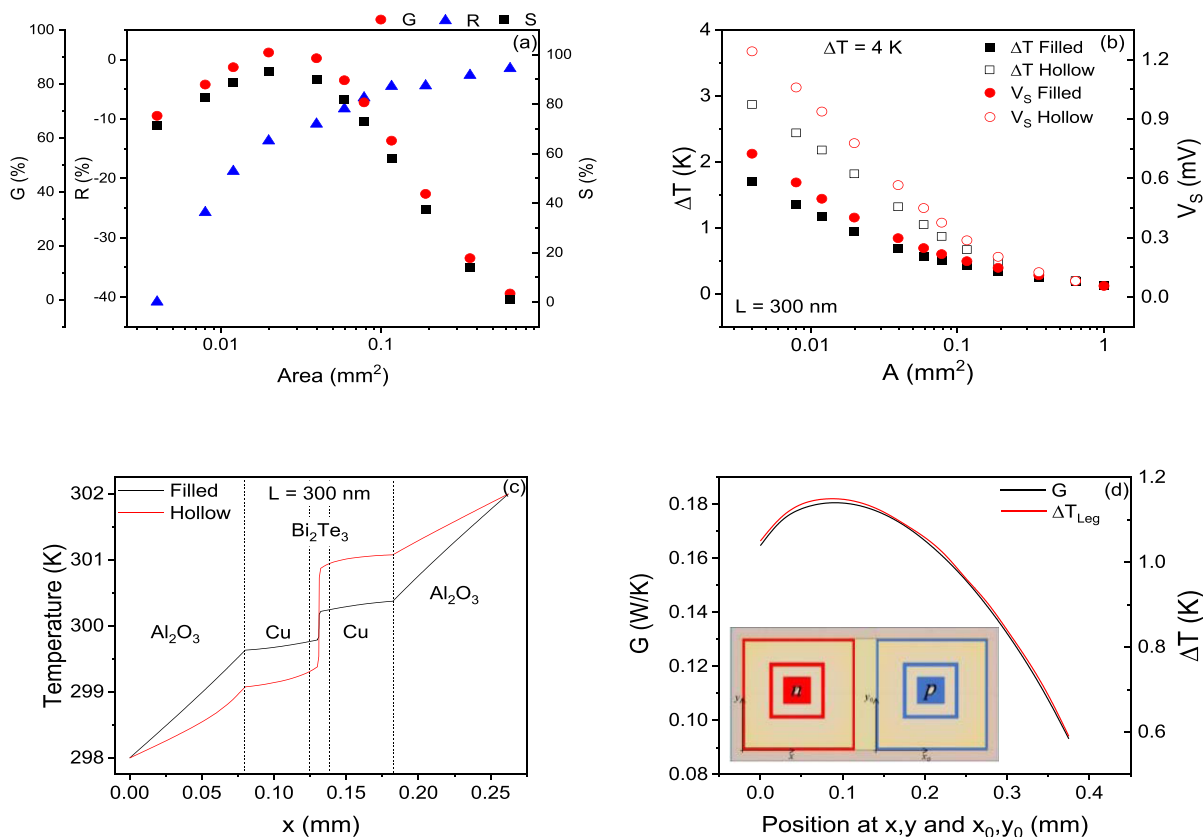
Figure 5. (a) Relative percentage increase for *G*, *R*, and *S* as a function of the cross-sectional area of the thermoelectric leg. (b) Temperature difference between the thermoelectric legs and Seebeck voltage generated by the devices as a function of the cross-sectional area of the filled and hollow geometries. (c) Temperature profile along the TEG with filled and hollow thermoelectric leg geometries. (d) Thermal conductance and temperature difference applied to thermoelectric legs as a function of the hollow thermoelectric leg position.

LeBlanc,[30] where a comprehensive summary of the main equations and modeling procedures related to COMSOL's thermoelectric module is presented.

3. RESULTS AND DISCUSSION

We simulated the device efficiency for several lengths of the thermoelectric legs with a fixed cross-sectional area of 0.19 mm^2. Figure 3a summarizes the results, where hollow devices tend to have higher output efficiencies. This is better summarized in Figure 3b, which shows the increase in the device efficiency in the hollow geometry by calculating the relative output efficiency $\eta_r = 100 \times \frac{\eta_{\text{hollow}} - \eta_{\text{filled}}}{\eta_{\text{filled}}}$. The maximum η_r is ca. 40% for lengths smaller than 500 nm, which means that a simple geometry optimization already produces outstanding results. It is worth mentioning that similar results were obtained when simulating the same structure/geometry with distinct materials, e.g., with PbTe$_2$ replacing Bi$_2$Te$_3$. Efficiencies were calculated from the simulated results of thermal conductance, internal electrical resistance, and Seebeck coefficient (see Figure S1 in Supporting Information for details).

We then kept the length of the thermoelectric legs fixed at 300 nm and simulated the thermal conductance (*G*), internal resistance (*R*), Seebeck coefficient (*S*), and the figure of merit (*ZT*), varying the cross-sectional area of the thermoelectric legs. Figure 4 shows that the device efficiency increases with decreasing cross-sectional area, as expected from the literature.[37] Indeed, a reduction in area causes the thermal

resistance to increase, thus optimizing the temperature difference between the thermoelectric legs. For large areas, the efficiency drops considerably, tending asymptotically to the same value, regardless of the geometry. The increase in the performance of TGEs with the hollow thermoelectric leg in Figure 4b shows a gain of more than 98%, for areas smaller than 0.0591 mm^2.

The increase in efficiency is more prominent in the hollow geometry at smaller cross-sectional areas (*A* < 0.1 mm^2), which is illustrated in Figure 5a for the relative percentage between the geometries for all thermoelectric parameters, i.e., $100 \times \frac{p_{\text{hollow}} - p_{\text{filled}}}{p_{\text{hollow}}}$, where *p* stands for thermal conductance, *G*; the internal resistance is *R*; and the Seebeck coefficient is *S*. The Seebeck coefficient (*S*) increases up to ca. 90% for devices with thermoelectric leg area between 0.01 and 0.04 mm^2, contributing to the increase in efficiency with the hollow geometry. Furthermore, the internal resistance decreases for hollow legs—reduction of approximately 20% for cross-sectional areas smaller than 0.012 mm^2, influencing on the efficiency of TEGs. In contrast, the thermal conductance has a maximum increase of ∼90% for hollow geometries for an area of the thermoelectric leg between 0.01 and 0.04 mm^2. Figure S2 in the Supporting Information compares the absolute values of *G*, *R*, and *S* for both geometries and several cross-sectional areas.

Studying the effects from the three parameters (*G*, *R*, and *S*) on the device efficiency is useful, but it does not allow us to understand the origin of the differences caused by geometry.
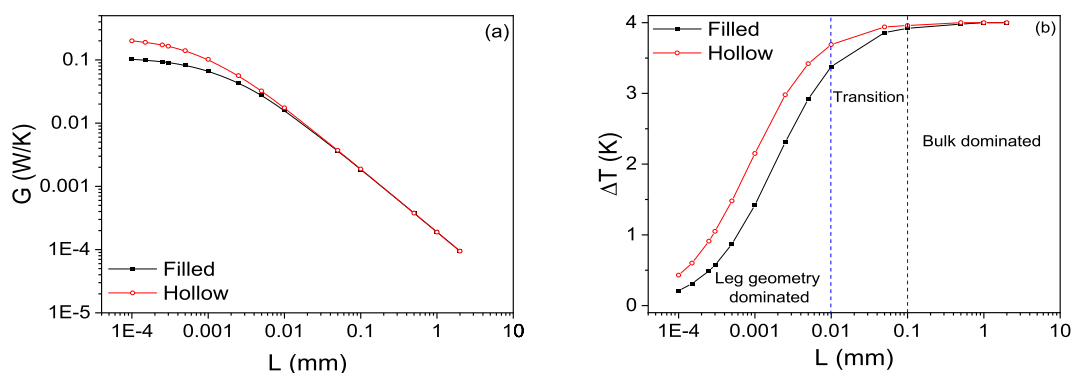
Figure 6. Thermal conductance (a) and temperature difference applied to the legs for TEGs (b) with filled and hollow thermoelectric legs with a cross-sectional area of 0.0591 mm^2, for several lengths of the thermoelectric legs.

Since the Seebeck coefficient depends on the Seebeck voltage ($S = V_S/\Delta T$), we decided to verify the importance of the temperature difference in the thermoelectric legs. Figure 5b shows that the temperature differences (ΔT_{Leg}) in the hollow devices are higher than those with filled geometry, and the same applies to the Seebeck voltage (V_S). This begs the question of why the temperature difference between the thermoelectric legs is larger for the hollow geometry if their thermal conductance is also higher. One should expect that a higher thermal conductance facilitates thermal equilibrium and generates smaller temperature differences. This apparent contradiction was resolved by investigating the temperature profile along the device. Figure 5c shows that for a fixed temperature difference of 4 K, the geometric differences between the filled and hollowed legs yield a distinct temperature distribution along the device. This increases the temperature gradient applied to the thermoelectric legs, even for high temperature differences, e.g., 100 K (for details, see Figure S3 in the Supporting Information). The results for the two geometries are the same, though, when the leg length is larger than 0.1, as shown in Figure S4. To explore further the apparent contradiction between thermal conductance and temperature difference, these parameters were simulated for TEG with hollow thermoelectric legs (L = 300 nm and A = 0.0591 mm^2), varying the position of the thermoelectric legs from the corner to the center of the electrical contact. This also changed the perimeter of the hollow thermoelectric leg. Figure 5d indicates that the position and perimeter of hollow thermoelectric legs affect thermal conductance and temperature difference applied to the thermoelectric legs. Both parameters reach a maximum when the thermoelectric leg is positioned around 0.1 mm from the corner of the electrical contact. Also, when the hollow thermoelectric legs become similar to filled thermoelectric legs (x,y position at 0.375 mm), the thermal conductance is the same for the two geometries (filled and hollow legs).

The increase in the efficiency occurs when the lengths of the thermoelectric legs are smaller than 0.1 mm, as indicated in Figure 3. Hence, it is also expected that the temperature difference applied to the thermoelectric leg and the device thermal conductance are the same for thermoelectric legs longer than 0.1 mm since thermal conductance dominates, and the influence of leg geometry becomes negligible. Figure 6a shows a higher thermal conductance for the hollow thermoelectric legs with lengths up to 0.05 mm and area of 0.0591 mm^2. For lengths smaller than 0.1 mm, the hollow geometry provides higher temperature differences, as shown in Figure 6b.

The influence from the temperature distribution along the TEGs caused by the thermoelectric leg geometry occurs when the influence of the thermoelectric leg length on the thermal resistance is no longer maximum. Also, the temperature difference tends to be a plateau for thermoelectric legs longer than 0.1 mm (dominance of thermal conductance).

It is worth mentioning that a similar trend was found when analyzing the simulated open-circuit voltage and output power curves for different leg geometries (see Figure S5 in the Supporting Information).

4. CONCLUSIONS

We have performed a systematic study of the influence from the thermoelectric leg geometry in thermoelectric generators with two commonly used geometries. For a fixed temperature difference of 4 K and a fixed cross-sectional area of 0.19 mm^2, a higher efficiency was observed for the thermoelectric generator with the hollow geometry, with a relative gain of ca. 40% for lengths smaller than 500 nm. The difference in efficiency was even higher (98%) in the hollow legs for the length of 300 nm and for cross-sectional areas smaller than 0.06 mm^2. In general, more efficient devices can be obtained by increasing the thermal resistance of a thermoelectric leg with an increase in its length and/or decrease in its cross-sectional area. Also, decreasing the temperature difference in the thermal and electrical contacts yields efficient TEGs. Although the thermal conductance is lower in the case of filled legs, the temperature applied to thermoelectric leg is higher in the case of hollow legs. Since the temperature difference applied to TEGs is fixed, the temperature distribution changes. This shows that for fabricating highly efficient miniaturized TGEs, one has to consider not only the thermal conductivity of the thermoelectric leg but also its geometry and temperature distribution along the device. The leg geometry is especially relevant for lengths smaller than 0.1 mm. As for bulker devices, the thermal conductance seems to be the dominating factor over the leg shape phenomena.

■ ASSOCIATED CONTENT

ⓢ Supporting Information

The Supporting Information is available free of charge at https://pubs.acs.org/doi/10.1021/acsomega.2c07916.

> Physical properties of all materials; relative percentage internal resistance considering the temperature; relative percentage increase for G, R, and S as a function of the thermoelectric leg length; G, R, and S of the TEGs as a

function of the thermoelectric leg cross-sectional area; temperature profile along the TEG when a temperature difference of 100 K is applied on the devices; temperature profile along the TEG with a thermoelectric leg length of 0.2 mm; open-circuit voltage and output power curves for the TEG with filled and hollow thermoelectric legs; and temperature profile along the hollow TEG measured at two different points of the hollow thermoelectric leg (PDF)

■ AUTHOR INFORMATION

Corresponding Author

Gustavo G. Dalkiranis − *São Carlos Institute of Physics, University of São Paulo, 13560-970 São Carlos, SP, Brazil; Catalan Institute of Nanoscience and Nanotechnology (ICN2), 08193 Barcelona, Spain;* orcid.org/0000-0001-9590-9249; Email: dalkiranis@gmail.com

Authors

João H. C. Bocchi − *São Carlos Institute of Physics, University of São Paulo, 13560-970 São Carlos, SP, Brazil*

Osvaldo N. Oliveira, Jr. − *São Carlos Institute of Physics, University of São Paulo, 13560-970 São Carlos, SP, Brazil;* orcid.org/0000-0002-5399-5860

Gregório C. Faria − *São Carlos Institute of Physics, University of São Paulo, 13560-970 São Carlos, SP, Brazil;* orcid.org/0000-0001-6138-8473

Complete contact information is available at:
https://pubs.acs.org/10.1021/acsomega.2c07916

Author Contributions

All authors have given approval to the final version of the manuscript.

Notes

The authors declare no competing financial interest.

■ ACKNOWLEDGMENTS

■ REFERENCES

(1) Demirbas, A. Global Renewable Energy Projections. *Energy Sources, Part B* **2009**, *4*, 212−224.

(2) Aklin, M.; Urpelainen, J. *Renewables: The Politics of a Global Energy Transition*; The MIT Press, 2018.

(3) Jaziri, N.; Boughamoura, A.; Müller, J.; Mezghani, B.; Tounsi, F.; Ismail, M. A Comprehensive Review of Thermoelectric Generators: Technologies and Common Applications. *Energy Rep.* **2020**, *6*, 264−287.

(4) Papapetrou, M.; Kosmadakis, G.; Cipollina, A.; La Commare, U. La; Micale, G. Industrial Waste Heat: Estimation of the Technically Available Resource in the EU per Industrial Sector, Temperature Level and Country. *Appl. Therm. Eng.* **2018**, *138*, 207−216.

(5) Ashraf, M.; Masoumi, N. A Thermal Energy Harvesting Power Supply With an Internal Startup Circuit for Pacemakers. *IEEE Trans. Very Large Scale Integr. (VLSI) Syst.* **2016**, *24*, 26−37.

(6) Bahk, J.-H.; Fang, H.; Yazawa, K.; Shakouri, A. Flexible Thermoelectric Materials and Device Optimization for Wearable Energy Harvesting. *J. Mater. Chem. C* **2015**, *3*, 10362−10374.

(7) Li, M.; Chen, J.; Zhong, W.; Luo, M.; Wang, W.; Qing, X.; Lu, Y.; Liu, Q.; Liu, K.; Wang, Y.; Wang, D. Large-Area, Wearable, Self-Powered Pressure−Temperature Sensor Based on 3D Thermoelectric Spacer Fabric. *ACS Sens.* **2020**, *5*, 2545−2554.

(8) Wang, L.; Zhang, K. Textile-Based Thermoelectric Generators and Their Applications. *Energy Environ. Mater.* **2020**, *3*, 67−79.

(9) Serrano-Claumarchirant, J. F.; Brotons-Alcázar, I.; Culebras, M.; Sanchis, M. J.; Cantarero, A.; Muñoz-Espí, R.; Gómez, C. M. Electrochemical Synthesis of an Organic Thermoelectric Power Generator. *ACS Appl. Mater. Interfaces* **2020**, *12*, 46348−46356.

(10) Mazzotta, A.; Carlotti, M.; Mattoli, V. Conformable on-skin devices for thermo-electro-tactile stimulation: materials, design, and fabrication. *Mater. Adv.* **2021**, *2*, 1787−1820.

(11) Yang, J. Potential Applications of Thermoelectric Waste Heat Recovery in the Automotive Industry. In *ICT 2005. 24th International Conference on Thermoelectrics*, 2005; pp 170−174.

(12) Hendricks, T. J. Integrated Thermoelectric-Thermal System Resistance Optimization to Maximize Power Output in Thermoelectric Energy Recovery Systems- CORRIGENDUM. *MRS Online Proc. Libr.* **2014**, *1642*, 1.

(13) Fitriani; Ovik, R.; Long, B. D.; Barma, M. C.; Riaz, M.; Sabri, M. F. M.; Said, S. M.; Saidur, R. A Review on Nanostructures of High-Temperature Thermoelectric Materials for Waste Heat Recovery. *Renewable Sustainable Energy Rev.* **2016**, *64*, 635−659.

(14) Rowe, D. M. *Thermoelectrics Handbook: Macro to Nano*; Taylor & Francis, 2005.

(15) Kroon, R.; Mengistie, D. A.; Kiefer, D.; Hynynen, J.; Ryan, J. D.; Yu, L.; Müller, C. Thermoelectric plastics: from design to synthesis, processing and structure-property relationships. *Chem. Soc. Rev.* **2016**, *45*, 6147−6164.

(16) He, R.; Schierning, G.; Nielsch, K. Thermoelectric Devices: A Review of Devices, Architectures, and Contact Optimization. *Adv. Mater. Technol.* **2018**, *3*, 1700256.

(17) Ferrando-Villalba, P.; Pérez-Marín, A. P.; Abad, L.; Dalkiranis, G. G.; Lopeandia, A. F.; Garcia, G.; Rodriguez-Viejo, J. Measuring Device and Material ZT in a Thin-Film Si-Based Thermoelectric Microgenerator. *Nanomaterials* **2019**, *9*, 653.

(18) Kim, H. S.; Liu, W.; Chen, G.; Chu, C.-W.; Ren, Z. Relationship between Thermoelectric Figure of Merit and Energy Conversion Efficiency. *Proc. Natl. Acad. Sci.* **2015**, *112*, 8205−8210.

(19) Snyder, G. J.; Toberer, E. S. Complex Thermoelectric Materials. *Nat. Mater.* **2008**, *7*, 105−114.

(20) Lee, G.; Choi, G.; Kim, C. S.; Kim, Y. J.; Choi, H.; Kim, S.; Kim, H. S.; Lee, W. B.; Cho, B. J. Material Optimization for a High Power Thermoelectric Generator in Wearable Applications. *Appl. Sci.* **2017**, *7*, 1015.

(21) Huen, P.; Daoud, W. A. Advances in Hybrid Solar Photovoltaic and Thermoelectric Generators. *Renewable Sustainable Energy Rev.* **2017**, *72*, 1295−1302.

(22) Sahin, A. Z.; Ismaila, K. G.; Yilbas, B. S.; Al-Sharafi, A. A Review on the Performance of Photovoltaic/Thermoelectric Hybrid Generators. *Int. J. Energy Res.* **2020**, *44*, 3365−3394.

(23) Culebras, M.; Gómez, C. M.; Cantarero, A. Review on Polymers for Thermoelectric Applications. *Materials* **2014**, *7*, 6701−6732.

(24) Chen, G.; Xu, W.; Zhu, D. Recent Advances in Organic Polymer Thermoelectric Composites. *J. Mater. Chem. C* **2017**, *5*, 4350−4360.

(25) Zheng, Y.; Liu, C.; Miao, L.; Li, C.; Huang, R.; Gao, J.; Wang, X.; Chen, J.; Zhou, Y.; Nishibori, E. Extraordinary Thermoelectric Performance in MgAgSb Alloy with Ultralow Thermal Conductivity. *Nano Energy* **2019**, *59*, 311−320.

(26) Soleimani, Z.; Zoras, S.; Ceranic, B.; Shahzad, S.; Cui, Y. A Review on Recent Developments of Thermoelectric Materials for Room-Temperature Applications. *Sustain. Energy Technol. Assessments* **2020**, *37*, 100604.

(27) Hasan, Md. N.; Wahid, H.; Nayan, N.; Mohamed Ali, M. S. Inorganic Thermoelectric Materials: A Review. *Int. J. Energy Res.* **2020**, *44*, 6170−6222.

(28) Liu, Z.; Liu, T.; Savory, C. N.; Jurado, J. P.; Reparaz, J. S.; Li, J.; Pan, L.; Faul, C. F. J.; Parkin, I. P.; Sankar, G.; Matsuishi, S.; Campoy-Quiles, M.; Scanlon, D. O.; Zwijnenburg, M. A.; Fenwick, O.; Schroeder, B. C. Controlling the Thermoelectric Properties of Organometallic Coordination Polymers via Ligand Design. *Adv. Funct. Mater.* **2020**, *30*, 2003106.

(29) Glatz, W.; Muntwyler, S.; Hierold, C. Optimization and Fabrication of Thick Flexible Polymer Based Micro Thermoelectric Generator. *Sens. Actuators, A* **2006**, *132*, 337−345.

(30) Thimont, Y.; LeBlanc, S. The Impact of Thermoelectric Leg Geometries on Thermal Resistance and Power Output. *J. Appl. Phys.* **2019**, *126*, 095101.

(31) Şişik, B.; LeBlanc, S. The Influence of Leg Shape on Thermoelectric Performance Under Constant Temperature and Heat Flux Boundary Conditions. *Front. Mater.* **2020**, *7*, 389.

(32) Shittu, S.; Li, G.; Zhao, X.; Ma, X. Review of Thermoelectric Geometry and Structure Optimization for Performance Enhancement. *Appl. Energy* **2020**, *268*, 115075.

(33) Min, G.; Rowe, D. M. Optimisation of Thermoelectric Module Geometry for 'Waste Heat' Electric Power Generation. *J. Power Sources* **1992**, *38*, 253−259.

(34) Kumar, S.; Heister, S. D.; Xu, X.; Salvador, J. R. Optimization of Thermoelectric Components for Automobile Waste Heat Recovery Systems. *J. Electron. Mater.* **2015**, *44*, 3627−3636.

(35) Vikhor, L. M.; Anatychuk, L. I.; Gorskyi, P. v. Electrical Resistance of Metal Contact to $Bi_2 Te_3$ Based Thermoelectric Legs. *J. Appl. Phys.* **2019**, *126*, 164503.

(36) Liu, Y.-L.; Liao, C.-N. Experimental and Theoretical Assessments of Thermal Boundary Resistance between $Bi_{0.4} Sb_{1.6} Te_3$ Thin Films and Metals. *Appl. Phys. Lett.* **2014**, *105*, 013903.

(37) Fan, L.; Zhang, G.; Wang, R.; Jiao, K. A Comprehensive and Time-Efficient Model for Determination of Thermoelectric Generator Length and Cross-Section Area. *Energy Convers. Manage.* **2016**, *122*, 85−94.